Steady-State and Transient Analysis of a CH_4–Catalytic Partial Oxidation Reformer

Ivan Tavazzi, Matteo Maestri, Alessandra Beretta, Gianpiero Groppi, Enrico Tronconi, and Pio Forzatti
Centro di Eccellenza per l'Ingegneria dei Materiali e delle Superfici Nanostrutturate (NEMAS, Center of Excellence for NanoEngineered Materials and Surfaces), Dipartimento di Chimica, Materiali e Ingegneria Chimica "Giulio Natta," Politecnico di Milano, 20133 Milan, Italy

DOI 10.1002/aic.10938
Published online July 14, 2006 in Wiley InterScience (www.interscience.wiley.com).

In this work dynamic and steady-state CH_4 partial oxidation tests, performed in an insulated lab-scale reactor over a Rh-based catalyst supported onto Al_2O_3 spheres, are presented and discussed. To gain insight in the complex observed phenomena a previously developed 1D heterogeneous mathematical model of adiabatic reactor was applied to data analysis. The model implemented an indirect reaction scheme independently derived in previous works. In experiments at low flow rates the heat dispersion significantly affected the steady-state response of the reactor; the process was governed by thermodynamics. By increasing the flow rate the catalytic bed progressively heated up and the adiabatic behavior was approached as a result of the predominance of the reaction enthalpy release over the heat losses; a kinetic effect of contact time was observed. Under these conditions start-up dynamics of the process were acquired. The temporal evolution of the product distribution along with the shape of axial temperature profiles at steady state were consistent with the occurrence of an indirect reaction path leading to the formation of synthesis gas. A sensitivity analysis showed that the description of the temperature profiles and conversion/selectivity performances at steady state is greatly influenced by the rate of the reforming reactions; the simulation of the reactor start-up dynamics is highly sensitive to the initial solid temperature. The comparison between measured temperature profiles and model predictions suggested that the thermocouple measurements were mainly influenced by the temperature of the flowing gas. © 2006 American Institute of Chemical Engineers *AIChE J,* 52: 3234–3245, 2006
Keywords: catalytic partial oxidation of CH_4, Rh/Al_2O_3 catalyst, insulated packed bed reactor, 1D dynamic model of CPO reformer

Introduction

The catalytic partial oxidation (CPO) of CH_4 represents a promising solution for the development of small- to medium-scale technologies of syngas and H_2 production. The possibility of operating at very short reaction times in simple and compact reactors and of using air as oxidant instead of pure O_2 makes this process suitable for stationary and mobile applications. H_2 generation for small distribution infrastructures, the fueling of H_2-fuel cells for residential power generation and of solid oxide fuel cells (SOFCs) for auxiliary power units (APUs) on heavy duty vehicles, the application of syngas in conventional internal combustion engine vehicles to improve the performances of engine, and catalytic converter during cold-starting are some proposed technologies.[1] Besides, the application of catalytic fuel-rich combustion of CH_4 was recently investigated in the literature to improve the performances of CH_4 combustors in advanced gas turbines.[2,3]

Schmidt and coworkers extensively investigated the partial oxidation of methane in short contact time reactors with dif-

Correspondence concerning this article should be addressed to A. Beretta at alessandra.beretta@polimi.it.

ferent catalyst supports[4-8]; they analyzed a number of important factors, including the effect of operating variables, the support geometry, and the nature of the catalyst. Because of the severe operating conditions that prevail in the reactor (with high flow rates and temperatures ranging from 700 to >1000°C), both intrinsic kinetics and transport phenomena affect the reactor behavior. For instance, Hohn and Schmidt[8] showed that the stability of small spheres against blow-out at high flow rates is higher than that of foams; indeed, because of lower heat transfer coefficients, the packed spheres are expected to be less sensitive to the quenching effect of the inlet flow.

A reliable description of the chemical process and the accurate modeling of the reactor are thus critical issues for process analysis and design. Deutschmann and coworkers[9,10] first addressed the detailed modeling of CH_4 partial oxidation over honeycomb catalysts and analyzed the combined effect of reaction kinetics and transport properties on the honeycomb performance.

In previous works the authors studied the kinetics of CH_4 partial oxidation over a low surface area 0.5% Rh/α-Al_2O_3 catalyst by using an isothermal annular reactor that operated at high space velocity[11-14] and developed a dynamic model of an adiabatic reactor that incorporated the derived molecular kinetics[15]; the model was applied to predict and compare the performances of fixed-bed reactors with different catalyst configurations (spheres, honeycomb, and foams). Model predictions pointed out the determining role played by transport phenomena, particularly by heat transfer properties, on the reactor behavior both at start-up and at steady state. Simulations evidenced that good interphase heat transport properties and low heat capacity (the typical features of foams) are useful for minimizing the total start-up time (ignition and propagation) but reduce the maximum flow rate at which an ignited steady state can be achieved and maintained.

In this work dynamic and steady-state CH_4 partial oxidation tests, performed in a lab-scale insulated reactor, are presented and discussed. Al_2O_3 spheres were adopted as catalyst support for simplicity. The analysis of the reactor thermal behavior was addressed, with the main goal of determining under which conditions the reactor operated quasi-adiabatically; a major effect of flow rate was found in this respect, in line with previous data from the literature.[16,17] Although most of the published data on methane CPO reformers deal with steady-state conditions, experimental efforts were herein devoted to analyze the dynamics of the reactor start-up and the effects of operating variables. To gain insight in the complex observed phenomena, the previously developed model was applied to data interpretation through the means of a sensitivity analysis.

Experimental

Catalyst

Partial oxidation of CH_4 was tested on a 0.5% (wt/wt) Rh/Al_2O_3 catalyst, obtained by grafting of $Rh_4(CO)_{12}$ dissolved in *n*-hexane[12,18] onto an Al_2O_3 support with BET surface area of about 40 $m^2\ g^{-1}$. The catalytic powders were wash-coated onto spheres of dense alumina with an average diameter of 3.4 mm according to the following procedure: a slurry was first prepared by ball milling the powders in an aqueous solution of HNO_3[19]; alumina spheres were dipped into the slurry and then flash dried at 240 °C to improve the mechanical resistance of the deposited catalyst layer. The coated spheres were finally treated in an ultrasound bath to eliminate catalyst excess possibly not well anchored to the surface.

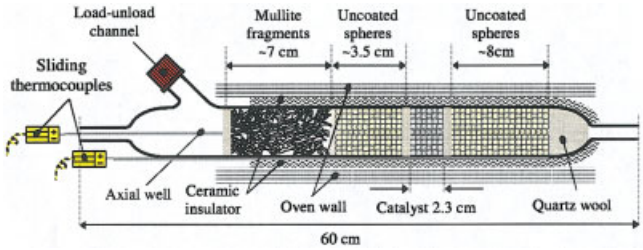

Figure 1. Lab-scale insulated reactor.

[Color figure can be viewed in the online issue, which is available at www.interscience.wiley.com]

Reactor setup

About 17 g coated spheres were packed in a tubular quartz reactor (internal diameter = 2.2 cm) to form a 2.3 cm long catalytic bed. The reactor assembly is sketched in Figure 1. The catalyst was placed between two beds of uncoated spheres, acting as thermal shields to prevent the axial heat dispersion by radiation. The upstream zone of the reactor was filled with mullite particles that helped both preheating of the flow of incoming reactants and its homogeneous distribution over the whole cross section. The reactor, equipped with an axial well for a sliding K-thermocouple (Ø 1 mm, 50 cm long), was wrapped in a layer (thickness ≈ 0.5 cm) of ceramic insulating material and placed inside a three-zone tubular oven. An additional sliding thermocouple, fixed by the insulating layer, was positioned outside the reactor in contact with the outer quartz wall and allowed to estimate peripheral gradients of temperature along the entire length of the bed. Tests were performed at atmospheric pressure with CH_4/air feeds (O_2/CH_4 ratio = 0.56).

Operating procedures

The start-up procedure consisted of first heating the catalyst to an initial temperature (380, 485, and 610°C) under static N_2 atmosphere (that is, with no flowing gas); during the reactor warmup, the calibrated CH_4/air mixture (at room temperature) was diverted in a by-pass line directly to the analysis section and composition of the reactants was measured. The mixture was then delivered to the reactor (time zero of start-up dynamics). CH_4, O_2, CO, CO_2, and H_2 outlet concentrations were dynamically measured with an in-line ABB AO2000 series continuous analysis system equipped with a condensation trap wherein the products stream was dried before entering the analyzers; H_2O was quantified by closing the balance of oxygen. Under steady-state conditions the analysis of the products composition was repeated by gas chromatography by which H_2O was also directly measured. Mass balances of converted C, H, and O were closed within a gap of 5%. The temporal evolution of temperature was recorded at different axial positions with repeated start-up/shut-down tests and, because of the imperfect reproducibility of initial thermal conditions along the whole reactor, slightly different transient responses were ob-

Table 1. Model Equations

Gas Phase

Species mass balance equations:
$$\frac{\partial \omega_i}{\partial t} = -\frac{G}{\rho_g \cdot \varepsilon}\frac{\partial \omega_i}{\partial z} - \frac{6(1-\varepsilon)}{d_p \varepsilon} K_{mat,i}(\omega_i - \omega_{i,\text{wall}})$$

Energy balance equation:
$$\frac{\partial T_g}{\partial t} = -\frac{G}{\rho_g \varepsilon}\frac{\partial T_g}{\partial z} - \frac{6(1-\varepsilon)}{d_p \cdot \varepsilon \cdot \rho_g \hat{c}_{p,g}} h(T_g - T_s) - \frac{4}{d_{rct}} h_{\text{oven}} \frac{1}{\rho_g \varepsilon \hat{c}_{p,g}} (T_g - T_{\text{oven}})$$

Momentum balance equation:
$$\left(-\frac{1}{\rho_g} + \frac{G^2}{\rho_g^2 \cdot p}\right)\frac{dp}{dz} - \frac{G^2}{\rho_g^2 \cdot T_g}\frac{dT_g}{dz} = \frac{1}{2}\frac{G^2}{\rho_g^2}\frac{6(1-\varepsilon)}{d_p} f$$

Solid Phase

Species mass balance equation:
$$0 = \frac{6(1-\varepsilon)}{d_p \varepsilon} \rho_g K_{i,mat}(\omega_i - \omega_{i,\text{wall}}) + \left(\sum_{j=1}^{NR} v_{i,j} r_j^{eff}\right) MW_i \rho_s \xi$$

Energy balance equation:
$$\frac{\partial T_s}{\partial t} = \frac{6(1-\varepsilon)}{d_p \varepsilon [\rho_s \hat{c}_{p,s}(1-\varepsilon)]} h(T_g - T_s) + \frac{1}{(\rho_s \hat{c}_{p,s})}\frac{\partial}{\partial z}\left(k_{ax}^{eff}\frac{\partial T_s}{\partial z}\right) + \left[\sum_{j=1}^{NR}(-\Delta H_j^R) r_j^{eff}\right] \xi / [\hat{c}_{p,s}(1-\varepsilon)]$$

Boundary Conditions

Reactor Inlet ($z_1 = 0$)

$$\omega_{i,z=z_1} = \omega_{i,\text{feed}}$$

$$T_{g,z=z_1} = T_{\text{room}} \qquad p_{z=z_1} = p_{\text{feed}}$$

$$-k_{ax}^{eff}\left.\frac{\partial T_s}{\partial z}\right|_{z_1} = \sigma \varepsilon_s (T_g^4 - T_s^4|_{z_1})$$

Reactor Outlet ($z_2 = L_{rct}$)

$$-k_{ax}^{eff}\left.\frac{\partial T_s}{\partial z}\right|_{z_2} = -\sigma \varepsilon_s (T_g^4 - T_s^4|_{z_2})$$

Initial Conditions

$$\omega_i(z, 0) = 0; \qquad T_g(z, 0) = T_{\text{room}}; \qquad T_s(z, 0) = T_{\text{oven}}$$

served, with a maximum deviation from the average start-up time lower than ±60 s. Data were elaborated by synchronizing the different runs to the average time, which allowed us to derive the dynamics of the axial temperature profile. At each preheating temperature [$T(t_0)$ in the following figures], several values of flow rate were tested from 35 to 240 NL h^{-1}.

The shut-down procedure consisted of progressively diluting the reactants mixture with N_2, at constant O_2/CH_4 ratio, to prevent thermal shocks of the reactor; eventually, the reactor was cooled to initial conditions by flowing pure N_2.

Reactor Modeling

In this work a previously developed 1D dynamic heterogeneous model of a fully insulated packed-bed reactor[15] was applied to data analysis. The model includes the species mass balances and the energy balances for the gas and solid phases, and the momentum balance for the gas phase. Model equations are reported in Table 1, whereas Table 2 summarizes the reactor and catalyst properties, as adopted in the model. It was not possible to obtain a reliable weight measurement of the catalyst amount deposited over the alumina spheres. Thus, a catalyst loading corresponding to a washcoat thickness of 20 μm with density equal to 1500 kg m^{-3} was assumed on the basis of previous results of dip coating over supports with a simpler geometry such as mullite tubes and metal plates.

To account for the preheating zone upstream from the catalyst, an additional heat transfer term was included in the enthalpy balance of the gas-phase by introducing an overall heat transfer coefficient, h_{oven}. Such a term accounts for the heat transfer between the oven and the reactor, that is, it accounts for the heating effect of the oven upstream from the catalyst and the dispersion from the reactor to the oven in the catalytic portion.

A value of 18 W m^{-2} K^{-1} for h_{oven} was determined independently by fitting the steady-state model simulations to experimental temperature profiles that were measured inside and upstream from the reactor under flowing N_2 under the same operating conditions (flow rates and oven temperatures) as those of the catalytic runs (Figure 2).

For the evaluation of the transport properties of the packed bed, the model incorporates state-of-the-art correlations and assumptions.[20-22] Thermal conduction in the solid phase was accounted for by means of an effective axial thermal conductivity[22] coefficient and in the solid-phase mass balance equations effective reaction rates were considered. The a-priori solution of the diffusion and reaction problem at a fixed reactor axial position (z) within the catalytic wash-coat indicated that the

Table 2. Reactor and Catalyst Properties Adopted in the Model

ρ_{cat} (kg m^{-3})	1500
ρ_{sphere} (kg m^{-3})	3800
$\hat{c}_p$ (kJ kg^{-1} K^{-1})	0.865
k_s (W m^{-1} K^{-1})	3
d_{rct} (m)	0.022
Upstream inert bed length (m)	0.12
Catalytic bed length (m)	0.023
d_{sphere} (m)	0.0034
Washcoat thickness (μm)	20
ε	0.48

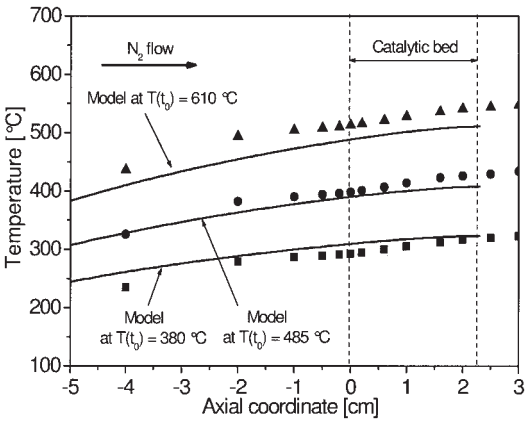

Figure 2. Steady-state *T* profiles measured in flowing N_2 (symbols) and model predictions (solid lines) with h_{oven} = 18 W m^{-2} K^{-1}.

Initial catalyst T = 380 °C (■), T = 485 °C (●), and T = 610 °C (▲); flow rate = 240 NL h^{-1}.

intraporous diffusive resistances for oxygen were greater by orders of magnitude than that for other species. Thus intraporous diffusive resistances were accounted for by an isothermal effectiveness factor only for combustion reactions, using the generalized Thiele modulus method.[23] Homogeneous reactions were neglected following the results reported in Schwiedernoch et al.[10] Given the high axial Péclet number, axial diffusion was neglected in the gas phase.

Kinetic scheme

In previous works,[11-14] an extensive series of experiments was devoted to the kinetic study of the partial oxidation of CH_4 over a Rh catalyst by performing catalytic tests in a structured annular reactor whose features allowed working at very short contact times, and thus out of thermodynamic control, under quasi-isothermal conditions. Experimental results were quantitatively analyzed with a 1D isothermal heterogeneous model. By studying the combined effects of temperature, contact time, and feed composition the prevalent stoichiometries of the reacting system were identified, thus reducing the complexity of the reaction network to a few main molecular reactions. An indirect kinetic scheme was proposed, consisting of a primary step of deep oxidation of CH_4 followed by secondary reactions of steam and CO_2 reforming of CH_4, responsible for the formation of synthesis gas, the reaction of water–gas shift, and the consecutive oxidations of H_2 and CO. Experiments evidenced that the rates of the oxidation and forward steam and CO_2 reforming are proportional to the concentration of CH_4 and independent of the partial pressure of coreactants. These results were in agreement with recent mechanistic studies by Iglesia and coworkers who investigated the steam and CO_2 reforming of CH_4.[24] The set of assumed reactions and developed rate expressions is summarized in Table 3. The approach to thermodynamic equilibrium of secondary reactions was accounted for by the factor $1 - \eta$ (where $\eta = K_P/K_{eq}$). Rate equations of combustion and reforming were multiplied by a factor defined as $\sigma_i = P_i/(10^{-6} + P_i)$ (where i = O_2, H_2O, and CO_2, respectively) to account for the rate-limiting effect of the coreactant in the case of complete consumption of species i. The kinetic parameters are listed in Table 4. The same kinetic scheme was adopted as a reference for a sensitivity analysis of the model responses, although the present catalyst differed from the catalyst originally used in the kinetic investigation because of a much higher surface area (40 vs. 4 m^2 g^{-1}).

Experimental Effects of Flow Rate and Inlet Temperature on the Thermal Efficiency

Initial efforts were devoted to identifying the experimental conditions that favored the approach to the desired adiabatic behavior. At this scope, tests were performed at increasing flow rate and varying preheating temperature. Figure 3 shows the evolution of the steady-state axial temperature profiles with increasing flow rate (initial catalyst temperature = 380°C). As observed in previous studies,[7,16] the measured temperature at the inlet catalyst section progressively decreased with increasing space velocity (as a result of the cooling effect of the incoming flow rate), whereas the outlet temperature increased. The present tests provided additional insight concerning the trend of the whole axial temperature profile, which gave kinetic information so far scarcely discussed in the literature; steady-state temperature profiles also represented a reference term for

Table 3. Stoichiometries and Rate Equations Included in the Indirect Kinetic Scheme

Methane combustion $CH_4 + 2O_2 \rightarrow 2H_2O + CO_2$	$R_{CTO} = \dfrac{k_{CTO} \cdot P_{CH_4}}{(1 + K_{ads,H_2O} \cdot P_{H_2O})^2}\,\sigma_{O_2}$
Steam reforming $CH_4 + H_2O \rightarrow 3H_2 + CO$	$R_{SR} = \dfrac{k_{SR} \cdot P_{CH_4} \cdot (1 - \eta_{SR})}{(1 + K_{ads,O_2} \cdot P_{O_2} + K_{ads,CO} \cdot P_{CO})^2}\,\sigma_{H_2O}$
CO_2 reforming $CH_4 + CO_2 \rightarrow 2H_2 + 2CO$	$R_{DR} = \dfrac{k_{DR} \cdot P_{CH_4} \cdot (1 - \eta_{DR})}{(1 + K_{ads,O_2} \cdot P_{O_2} + K_{ads,CO} \cdot P_{CO})^2}\,\sigma_{CO_2}$
Rev. water–gas shift $CO_2 + H_2 \rightarrow CO + H_2O$	$R_{RWGS} = \dfrac{k_{RWGS} \cdot P_{CO_2} \cdot P_{H_2} \cdot (1 - \eta_{RWGS})}{(1 + K_{ads,O_2} \cdot P_{O_2} + K_{ads,CO} \cdot P_{CO})^2}$
CO oxidation $CO + 0.5O_2 \rightarrow CO_2$	$R_{Ox,CO} = k_{Ox,CO} \cdot P_{CO} \cdot \sigma_{O_2}$
H_2 oxidation $H_2 + 0.5O_2 \rightarrow H_2O$	$R_{Ox,H_2} = k_{Ox,H_2} \cdot P_{H_2} \cdot \sigma_{O_2}$

Table 4. Kinetic and Adsorption Parameters (Constants Reported at 773 K) Derived in the Original Kinetic Study*

	Reaction							Adsorption		
	TO	SR	DR	RWGS	Ox, H_2	Ox, CO		O_2	H_2O	CO
k^{773K}	0.0029	0.0022	0.0022	0.34	2	0.09	K_{ads}^{773K}	120	4.2	23.8
E_{att}/R	6800	7100	7100	3900	5000	7000	$-\Delta H_{ads}/R$	7000	19,900	3100

*TO, total oxidation; SR, steam reforming; DR, dry reforming; RWGS, reverse water–gas shift; Ox, CO (H_2), CO (H_2) oxidation. $[k_j]$ = mol s^{-1} g_{cat}^{-1} atm^{-1}; $[k_{RWGS}]$ = mol s^{-1} g_{cat}^{-1} atm^{-2}; $[K_{ads}]$ = atm^{-1}; $[E_{att}/R] = [\Delta H_{ads}/R] = [K]$.

the analysis of start-up dynamics. The occurrence of a temperature maximum was systematically observed, corroborating the assumption of an exothermic–endothermic reaction sequence within the reactor; by increasing the space velocity, the temperature peak gradually shifted toward the center of the catalytic bed (an effect of the convective heat transfer) and the hot-spot temperature increased. This trend was associated with the improved efficiency of the thermal insulation, as a consequence of the lower relative relevance of heat dispersions at increasing enthalpy fluxes.

To evaluate the approach to the adiabatic behavior, the experimental setup was schematically treated as an ideal-sequence preheater/reactor; the aim of the analysis was a comparison between the adiabatic and the real temperature increase across the "reactor" portion. In each test, the "reactor" inlet temperature (that is, the "preheater" outlet temperature) was conventionally assumed as the temperature T_{N2}^{IN} that established and was measured in the catalytic bed in the absence of any reaction, under flowing N_2, at the same flow rate and oven temperature used in the catalytic experiment. Thus, the measured temperature increase was evaluated as

$$\Delta T_{exp} = (\text{measured outlet temperature} - T_{N2}^{IN})$$

and the thermal efficiency α of the reactor was defined as

$$\alpha = \Delta T_{exp}/\Delta T_{adiab}$$

where ΔT_{adiab} represents the calculated temperature rise of an adiabatic reactor at the observed outlet composition.

Values of α at varying flow rates and initial catalyst temperatures are reported in Figure 4. At low flow rates, α was significantly <1, which indicates the major role of heat dispersion on the reactor performances. By increasing the flow rate, α progressively increased and approached unity at the highest space velocity and the lowest preheating temperature investigated. Notice that under this condition peripheral temperature gradients, and thus heat dispersion, were still present: the gap between the measures of temperature inside and outside the reactor was in fact in the range of 50–75°C. However, the enthalpy flux released by the reaction became increasingly significant with respect to dispersion effects, which allowed us to identify operating conditions of high thermal efficiency of the reactor relevant for the model analysis.

Figures 5 and 6 show the experimental combined effect of flow rate and inlet temperature on the steady-state CH_4 conversion and selectivity to synthesis gas, respectively, along with thermodynamic predictions calculated at the outlet measured temperature. Similar effects were previously reported in the literature, but they are discussed herein in relation to the thermal efficiency of the reactor and represent a reference for the dynamic modeling. It is worth mentioning, as better illustrated in the following, that, according to model predictions, in the range of investigated space velocities the gas-phase temperature equals the catalyst temperature in the outlet reactor section; thus, measured outlet temperatures represent proper references for thermodynamic analysis. At lower space velocity the process was governed by thermodynamics. Thus, contrary to the trends observed in the annular reactor under chemical control and isothermal conditions, CH_4 conversion and syngas selectivity grew with increasing flow rate as a result of the progressive heating of the reactor associated with the in-

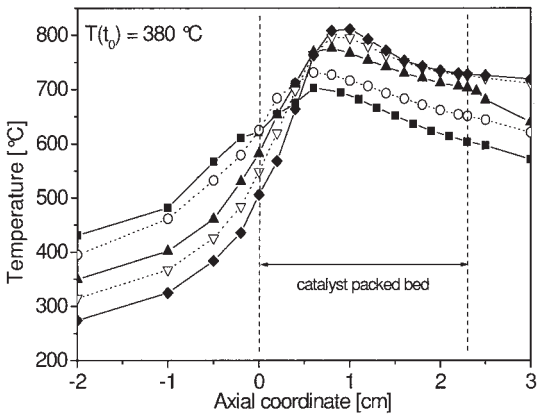

Figure 3. Axial temperature profiles measured along the axial coordinate in experiments with an initial catalyst T = 380 °C at flow rates of 35 (■), 70 (○), 136 (▲), 192 (▽), and 240 (◆) NL h^{-1}.

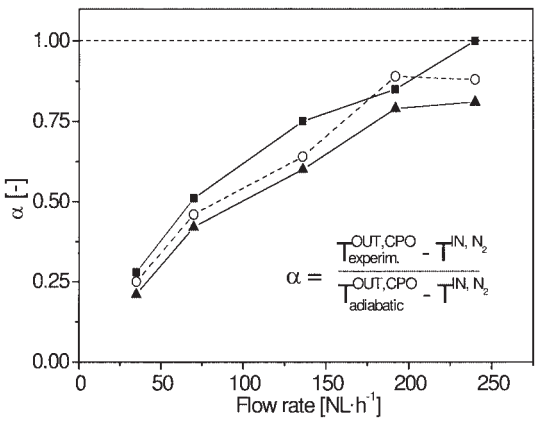

Figure 4. Measured trend of the thermal efficiency $\alpha = \Delta T/\Delta T_{adiabatic}$ vs. flow rate at preheating temperature (T) = 380 °C (■), T = 485 °C (○), and T = 610 °C (▲).

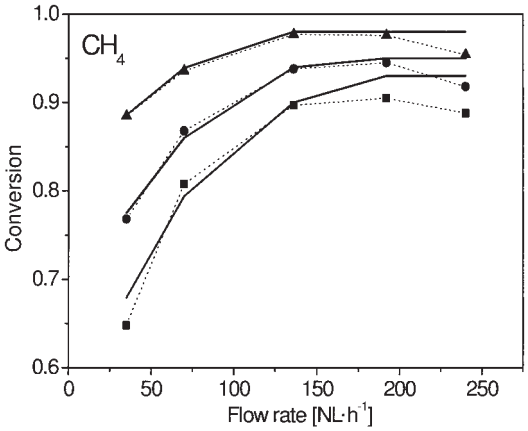

Figure 5. CH_4 conversion vs. flow rate at preheating temperature (T) = 380 °C (■), T = 485 °C (●), and T = 610 °C (▲).

Measured data (symbols) are compared to equilibrium values (solid lines). Feed: O_2/CH_4 = 0.56.

creasing thermal efficiency. Besides, the effect of contact time was significantly stronger on CO selectivity than on H_2 selectivity, reflecting the trend with the temperature of the respective equilibrium values at the outlet temperatures investigated. Only at very high space velocity, once a quasi-adiabatic behavior was reached, a kinetic effect of contact time was observed because CH_4 conversion tended to decrease and the approach to the equilibrium weakened. O_2 conversion was always complete. High flow rate conditions were identified as the most kinetically informative and, thus, the most interesting for reactor modeling.

The single effect of the preheating temperature can be appreciated from the data in Figure 7. In line with previous studies, a slight increase of CH_4 conversion and syngas selectivity was observed with increasing temperature. The corresponding measured temperature profiles are shown in Figure 8. The measured hot-spot temperature grew from about 800 to 900 °C and was located at about one third of the reactor length. The outlet temperature increased only moderately from about 750 to about 800°C; the scarce sensitivity of the outlet temperature toward changes of the inlet temperature is related to the self-adjusting thermal behavior of the reactor, wherein major changes of the inlet temperature are substantially compensated by small changes of the methane conversion and syngas selectivity.

Dynamics of Startup

Figure 9a shows the evolution of the axial temperature profile measured after the injection of the feed stream at the preheating temperature of 380°C. At the initial stage (within 4 min from time zero), a hot spot slowly formed at the back end of the catalytic bed. Afterward, the hot spot grew faster and propagated upstream throughout the entire catalyst bed. Within 7.5 min, the hot-spot temperature had reached its steady-state location and value.

Regarding the product mixture, after feeding the reactants an induction time of about 4 min was observed, corresponding to the initial formation of the hot spot; in this phase, O_2 and CH_4 concentrations decreased very little with time with unique formation of H_2O and CO_2 (Figure 10). Ignition then occurred and the conversion of reactants sharply increased (the conversion of O_2 reached 100%); correspondingly, the net production of H_2O and CO_2 grew to a considerable extent and was accompanied by the rapid formation of H_2 and CO. The concentration of deep oxidation products passed through a maximum, whereas the concentration of the partial oxidation products sharply increased with time. After ignition was completed a slight cooling of the inlet catalyst portion was observed accompanied by a slow decrease with time of methane conversion and synthesis gas production.

At the preheating temperature of 610 °C (Figure 11), no induction time was observed and an instantaneous fast evolution of the process occurred immediately after injection of the feed stream. The measured outlet concentration of O_2 dramatically decreased, approaching zero within about 2 min. Similarly, the concentration of CH_4 reached the final steady-state value within a few minutes. H_2O, CO_2, H_2, and CO were observed in the product mixture from the very beginning; again, the concentrations of H_2O and CO_2 passed through maxima, whereas the concentration of synthesis gas grew with time.

The detection of O_2 among the reaction products in the early

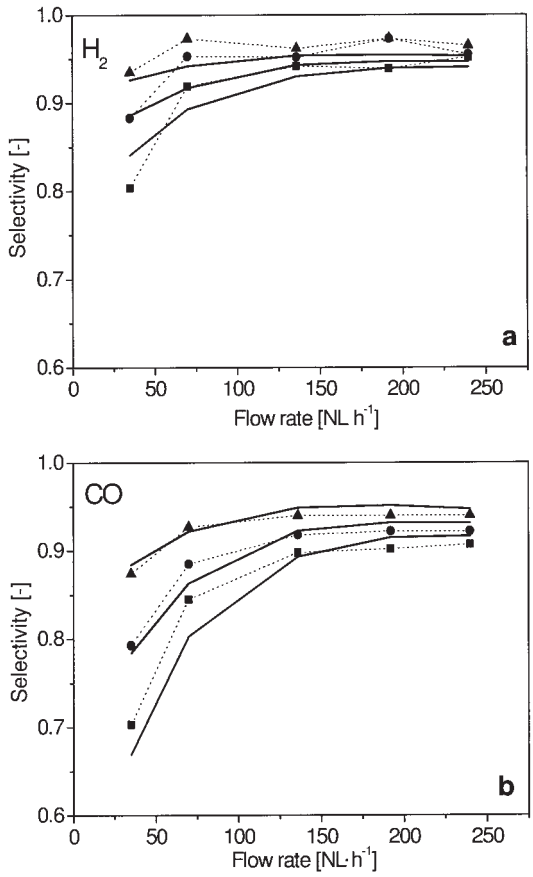

Figure 6. (a) H_2 selectivity and (b) CO selectivity vs. flow rate at T = 380 °C (■), T = 485 °C (●), and T = 610 °C (▲).

Measured data (symbols) are compared to equilibrium values (solid lines). Feed: CH_4/air, O_2/CH_4 = 0.56; 1 atm.

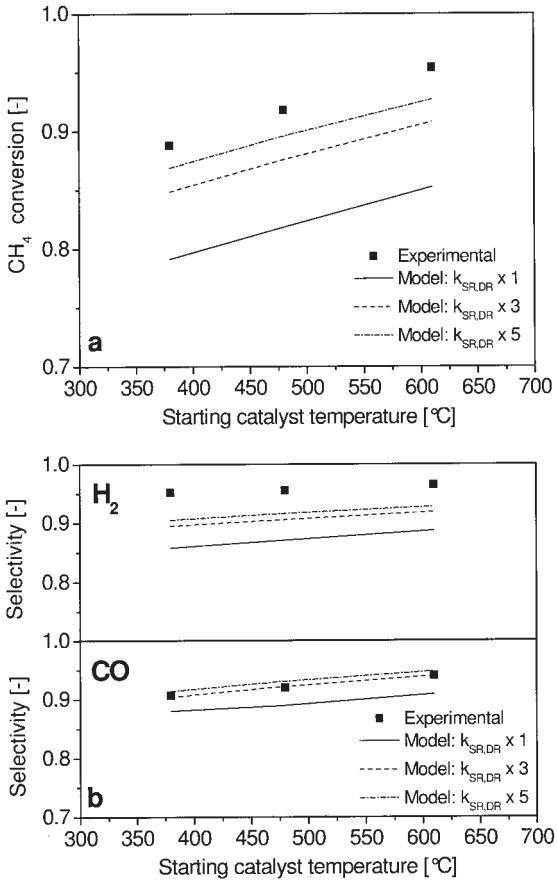

Figure 7. Comparison between model predictions (solid line) and experimental data (■).

(a) CH_4 conversion at steady state; (b) selectivity to H_2 and CO at steady state vs. the preheating temperature. Flow rate = 240 NL h^{-1}.

transient phase was hardly feasible, given the high preheating temperature of the catalyst, as confirmed by model simulations, discussed in detail below, which predicted a total consumption of oxygen since the very initial stages of the light-off dynamics. On the basis of these considerations the transient response of the continuous analyzer to sudden variations of the mixture composition was tested; an air/N_2 flow was delivered to the analysis system through the by-pass line in experiments wherein step variations of O_2 concentration were imposed by means of a digitally controlled mass flow controller. For a step change of oxygen concentration from 15 to 0% the response of the analyzer was practically coincident with that recorded during the catalytic experiment, as shown in the comparison reported in the inset of Figure 11a. Consequently, the observed light-off dynamics actually corresponded to an instantaneous complete depletion of O_2. The estimation of the effect of response delay on the other gas species is more complex because their actual concentration does not instantaneously reach a constant value. Further investigation and modeling are presently ongoing to account for such effects on the analyzer output. In Figures 11b–11f the complete dynamics are shown as provided by the acquisition system; nonetheless, we note that data at times <60 s could correspond to unreliable values. Given the rapidity of the dynamics, the evolution of the temperature measurements was considered unreliable and was not recorded.

Model-based Analysis

The reactor performances at the high flow rate of 240 NL h^{-1} (under quasi-adiabatic behavior) were simulated by the 1D model. A sensitivity analysis allowed us to identify some key parameters that greatly influence the description of both the steady-state and the dynamic behaviors.

Concerning the effect of the preheating temperature on the steady-state conversion and selectivity, it was found that the model responses were greatly affected by the assumed intrinsic rates of secondary reactions. Figure 7 compares the experimental results with simulations wherein the kinetic constants of steam and dry reforming were parametrically varied with respect to the reference set of rate parameters. At adopting the parameters of the original kinetic study, model simulations tended to underestimate the CH_4 conversion and the syngas selectivity. By increasing both the rates of steam and CO_2 reforming by a factor of either 3 or 5, while keeping all the other parameters unchanged with respect to those reported in Table 4, a satisfactory match was found. As shown in Figure 8, upon increasing the rate of both endothermic reactions, the calculated outlet temperatures of the solid phase and gas phase

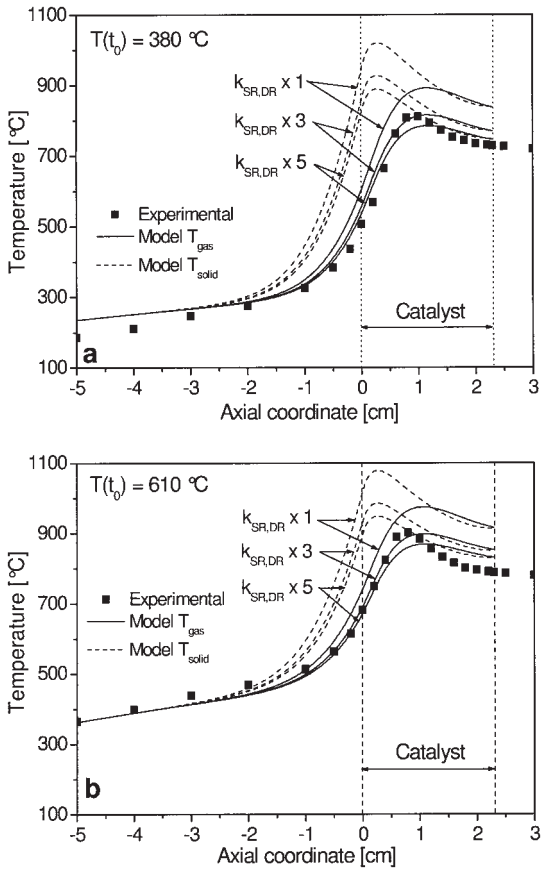

Figure 8. Steady-state axial temperature profiles.

Experimental measurements (symbols) vs. model predictions of gas (solid line) and solid (dashed line) temperature; flow rate = 240 NL h^{-1}; at (a) $T(t_0)$ = 380 °C and (b) $T(t_0)$ = 610°C.

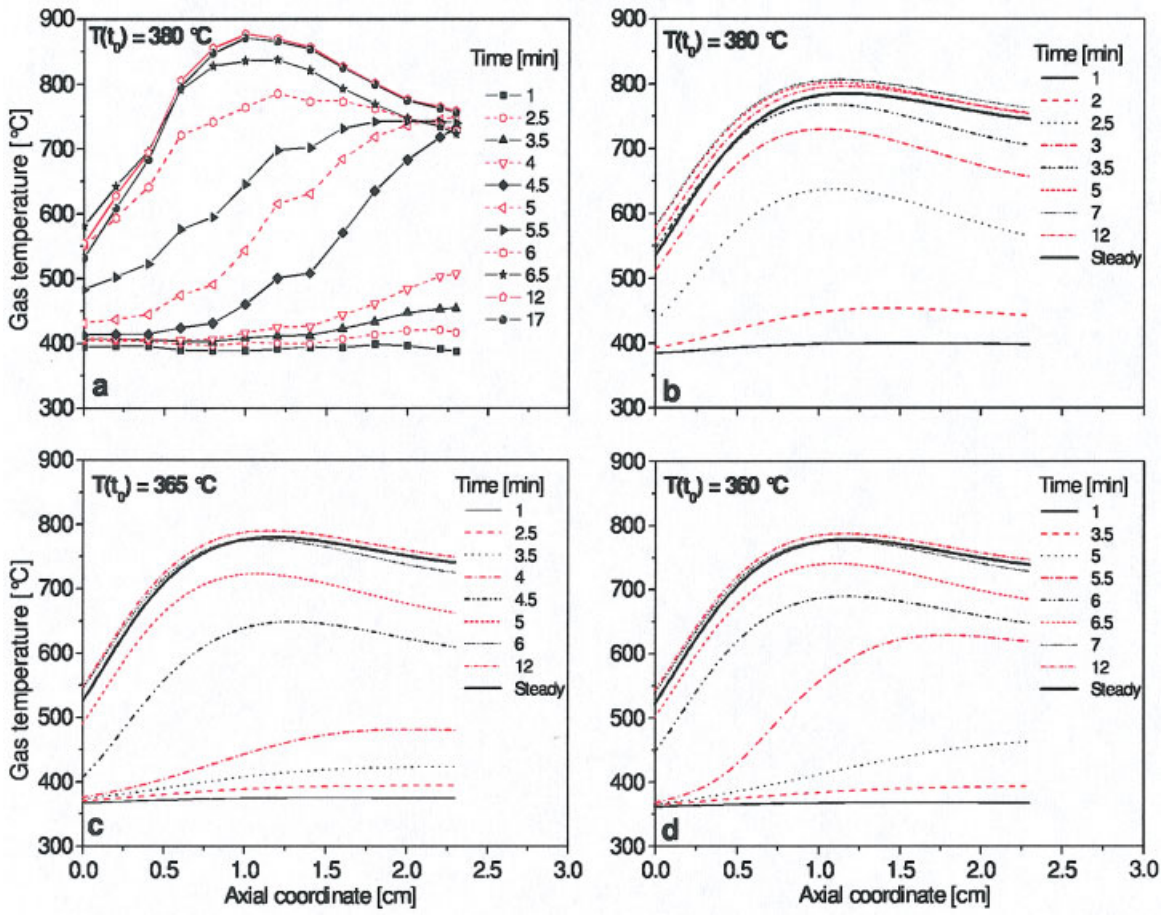

Figure 9. (a) Experimental and (b) calculated dynamics of the gas-phase temperature profile during the start-up with T = 380°C. (c) and (d) Calculated dynamics with preheating temperatures of 365 and 360°C.

Flow rate = 240 NL h^{-1}. [Color figure can be viewed in the online issue, which is available at www.interscience.wiley.com]

decreased significantly and more closely approached the measured outlet temperatures. A quantitative and qualitative (such as the same axial location of the hot spot) analogy was evident between the thermocouple measurements and the predicted gas-phase profiles, which suggests that the thermocouple was equilibrated with the flowing gas temperature. This probably depends on the distribution of the packing around the thermocouple. In fact, in the present reactor setup, the void fraction was close to 0.50, which likely hindered the contact between the thermocouple and the catalyst particles. Indeed, other experiments performed with a Pd catalyst, smaller spheres, and a lower bed void fraction gave rise to much sharper measured profiles, closer to the calculated solid-phase temperature.

Concerning the start-up dynamics, contrary to measurements, the model simulated an initial distributed heating of the catalyst bed (independently of the value assumed for the kinetic constants of the reforming reactions), with fast formation of a hot spot in the middle of the catalytic bed that rapidly grew and approached steady-state conditions within about 5 min (Figure 9b). However, the predicted dynamics exhibited a high sensitivity toward the assumed preheating temperature. Figures 9c and 9d compare the results of simulations wherein the initial reactor (inert + catalyst) temperature was set at 365 and 360°C. In the latter case, the qualitative agreement with the experimental trend was recovered: the thermal dynamic behavior corresponded in fact to a back-end ignition. However, the approach to steady state was significantly delayed. At the intermediate preheating temperature of 365°C, an intermediate trend (the hot spot formed close to the back end) and intermediate characteristic times were found. As a general comment, it is interesting to note that the observation of the initial formation of a hot spot followed by its rapid growth was confirmed from the model simulations. To better understand this trend, it should be recalled that the kinetics of CO and H_2 postcombustions are much faster than the kinetics of methane combustion; thus, during start-up, once the catalyst bed temperature is sufficiently high to activate the steam and dry reforming reactions, a propellant effect on O_2 consumption (and on the reactor heating) initially occurs as a result of the consecutive oxidations of H_2 and CO; only after complete consumption of O_2 is synthesis gas observed in the product mixture in a significant amount.

The temporal evolution of the calculated product distribution (Figure 10) was very close to the experimental trend; of course, the predicted dynamics reflected the faster evolution of the calculated temperature profiles. By considering progressively lower preheating temperatures, the reactor light-off was accordingly delayed and a closer description of the experiments was obtained. The best match was provided by the simulations at 365°C. Note that temperatures were acquired with an uncer-

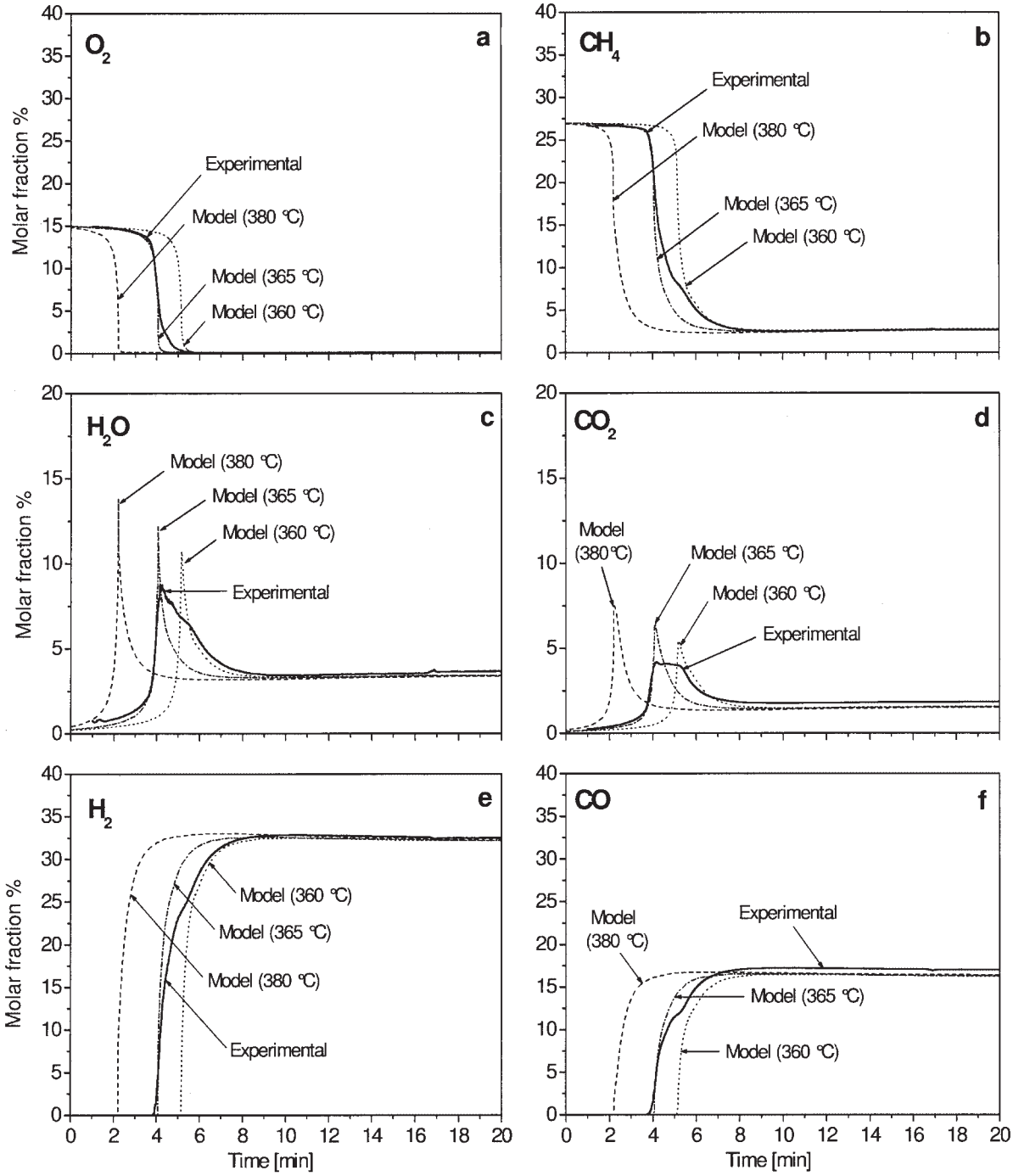

Figure 10. Comparison between experimental data [$T(t_0) = 380°C$] and model predictions [$T(t_0) = 380$, 365, and 360°C] of the dynamics of the outlet mixture composition during the process start-up at flow rate = 240 NL h^{-1}.

tainty of ±5°C, which makes relevant the difference between the measured preheating temperature and that required to fit model predictions to observed data.

At the high preheating temperature of 610°C, in line with the experimental evidence, the model predicted the instantaneous complete conversion of oxygen (Figure 11). The consumption of methane and the concentration of all the reaction products were also significant at time zero and grew rapidly within about 3 min. The predicted trends were qualitatively in line with the experiments, but the various observed dynamics were slightly slower. An inspection of the calculated reactor temperatures was useful to better comprehend the reasons for the rapid start-up; as shown in Figure 12a, a hot spot formed immediately after injection of the feed stream (according to a mechanism of front-end ignition) and a time period of 30 s was sufficient to obtain gas-phase temperatures > 700 °C along the entire reactor length. This is explained by the fact that under these conditions (that is, at high initial solid temperature), the reaction rates were so high that the whole

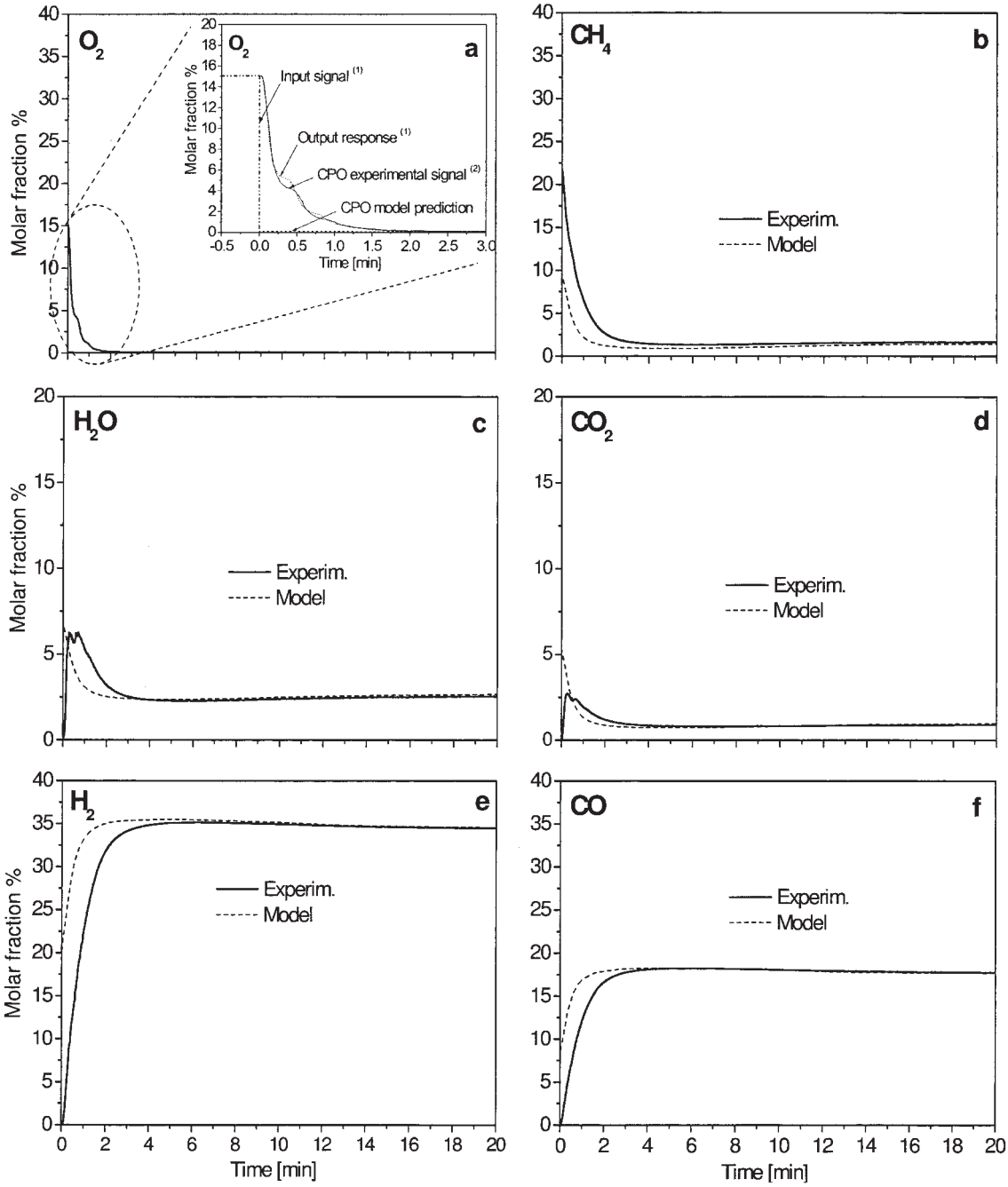

Figure 11. Comparison between experimental data and model predictions of the dynamics of the outlet mixture composition during the process start-up at $T(t_0)$ = 610 °C and flow rate = 240 NL h^{-1}.

Inset in (a): (1) Input signal and output response of the analyzer for a step variation of O_2 concentration. (2) O_2 dynamics measured during the catalytic run.

process was greatly accelerated. In particular, the rate of methane combustion was sufficiently high to cause the complete conversion of the incoming O_2 flow, which in turn initiated an escalation of the temperature increase and a rapid change of the product composition. Notably, after about 4 min from start-up, the reactor had reached the maximum values of temperature; these slowly decreased during the following 10 min until the steady-state profile was established. Such behavior was already observed at lower preheating temperature (380°C) and was more pronounced at high temperature. Consistently, the distribution of products after the ignition slowly changed (Figure 11); the consumption of methane and, consequently, the production of H_2 and CO slightly decreased with time. As better shown in Figure 12b, this cooling effect arises from the slow equilibration of the inert volume in front of the catalytic bed, externally heated by the oven and quenched by the cold feed stream; such behavior was experimentally confirmed by measurements of temperature profiles carried out after completion of the fast light-off dynamics.

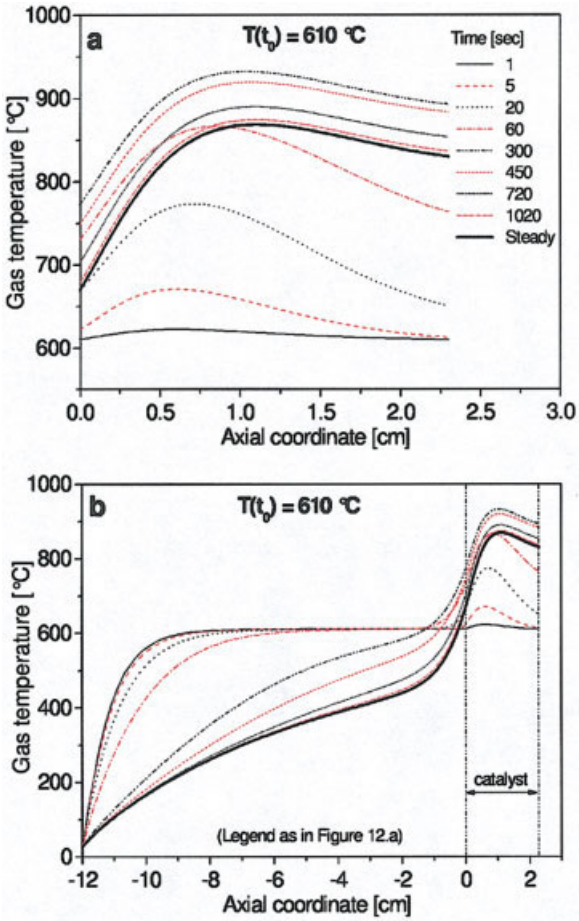

Figure 12. Calculated dynamics of the gas-phase axial temperature profile during the start-up with preheating temperature = 610°C.

(a) Catalyst bed length; (b) inert bed + catalytic bed total length. [Color figure can be viewed in the online issue, which is available at www.interscience.wiley.com]

Conclusions

The process of catalytic partial oxidation of methane was studied in an insulated lab-scale packed-bed reactor. Several findings emerged from the experimental work as well as from the model based analysis.

- The thermal efficiency of the reactor, herein evaluated in terms of $\alpha = \Delta T_{exp}/\Delta T_{adiab}$, was greatly enhanced by increasing the total flow rate. At the highest investigated flow rate of 240 NL h^{-1}, heat losses became negligible and the reactor could be reasonably treated as an adiabatic reactor. Also, under short contact time operation, the product distribution was not fully governed by thermodynamics. Both factors concurred to identify the conditions of high flow rate as those most suitable for analyzing the steady-state and transient performances of the reformer.
- The previous proposal of an indirect kinetic scheme to synthesis gas over Rh catalyst derived under isothermal conditions was confirmed by the present CPO tests. The steady-state axial temperature profiles were characterized by the presence of a pronounced hot spot at the entrance of the reactor, which is in line with the existence of an exothermic–endothermic reaction sequence. Besides, the temporal evolution of products observed during the start-up dynamics corroborated the proposal that CO_2/H_2O and CO/H_2 are, respectively, primary and secondary reaction products.
- The previously developed one-dimensional heterogeneous model of an adiabatic reformer was adapted to describe the actual experimental apparatus; the presence of an inert bed upstream from the catalyst was accounted for by assuming a stepwise activity profile, whereas the presence of the oven was accounted for through an overall heat transfer term, independently estimated. By introducing an independently derived kinetic scheme, transient and steady-state model simulations showed a qualitative agreement with all the main reformer features (such as shape of the steady-state temperature profiles, effect of inlet temperature on conversion/selectivity, and dynamics of the product mixture during start-up).
- Heat and mass transfer, as well as the chemical reaction, govern the performance of a short contact time reformer. Accordingly, the description of the reactor is expected to be highly sensitive to several kinetic and transport properties. In this work, we have first analyzed the sensitivity toward the chemical reaction. At this scope, a basis was provided by the kinetic scheme that, in other works, was derived for a low surface area Rh catalyst (although different from the formulation herein tested). It was found that the steady-state performance of the reformer is dramatically influenced by the rate of secondary reactions, whose extent controls both the reactor thermal behavior and the product composition. With respect to the start-up dynamics, the temporal evolution of the temperature profiles and of the product distribution is greatly influenced by the assumed initial solid temperature; in turn, this parameter controls the initial methane combustion rate, which represents the governing driver of ignition.
- Model analysis provided a useful tool for a better comprehension of several experimental observations. In the present reactor arrangement, model calculations evidenced the influence of the gas-phase temperature on the thermocouple measurements. This implies that the actual solid temperature was much higher than the measured temperature profile, especially in the inlet zone, where the hot spot was located; the nonconservative nature of the thermocouple measurements represents an important warning for a safe and stable reactor operation (metal volatilization or sintering are expected to affect the catalyst stability at high temperatures).

Moreover, the calculated temperature dynamics allowed us to better interpret the observed evolution of the product mixtures during start-up, thus supporting or even replacing the direct (but in some cases unreliable) measurements. Both experiments and simulation trends showed that the reactor light-off passes through an initial ignition, during which methane combustion starts the reactor heating, followed by a rapid propagation that completes the conversion of O_2 and is accelerated by the initial formation of synthesis gas. With increasing initial catalyst temperature, the light-off mechanism shifts from a back-end path (experimentally observed) to a front-end path. Indeed, at a sufficiently high preheating temperature, the inlet reactor zone rapidly consumes the incoming O_2 flow without any ignition delay.

Acknowledgments

The authors gratefully acknowledge the financial support provided by MIUR-Rome, EU Cathlean Project, and Center for NanoEngineered Materials and Surfaces.

Notation

A = reactor cross section, m^2
$\hat{c}_p$ = specific heat, J kg^{-1} K^{-1}
d_p = sphere diameter, m
f = friction factor
G = superficial mass flow rate, kg m^{-2} s^{-1}
MW = molecular weight, kg mol^{-1}
h = heat transfer coefficient, W m^{-2} K^{-1}
k_{ax}^{eff} = effective solid thermal conductivity, W m^{-1} K^{-1}
$K_{mat,i}$ = mass transfer coefficient, m s^{-1}
L_{rct} = reactor length, m
p = pressure, Pa
r_j = j^{th} reaction rate, mol kg_{cat}^{-1} s^{-1}
t = time, s
T = temperature, K
z = reactor axial coordinate, m

Greek letters

ε = bed void fraction
ε_s = emissivity
ΔH_j^R = heat of reaction, J mol^{-1}
ξ = volumetric catalytic fraction
ρ = density, kg m^{-3}
σ = Stefan–Boltzmann constant, K^{-4}
ω = weight fraction

Subscripts and superscripts

1 = inlet section of the inert bed
2 = outlet section of the catalytic bed
g = gas phase
s = solid phase
eff = effective

Literature Cited

1. Basini L. Fuel rich catalytic combustion: Principles and technological developments of SCT catalytic processes. In Forzatti P, Groppi G, Ciambelli P, Sannino D, eds. *Catalytic Combustion*. Volume 1. Milan, Italy: Polipress; 2005:7-11.
2. Lyubowsky M, Smith LL, Castaldi M, Karim H, Nentwick B, Etemad S, LaPierre R, Pfefferle WC. Catalytic combustion over platinum group catalysts: Fuel-lean versus fuel-rich operation. *Catal Today*. 2003;83:71-84.
3. Smith LL, Castaldi MJ, Etemad S, Pfefferle WC. Fuel-flexible fuel-rich catalytic combustion with ultra-low emissions. In Forzatti P, Groppi G, Ciambelli P, Sannino D, eds. *Catalytic Combustion*. Volume 1. Milan, Italy: Polipress; 2005:55-60.
4. Hickman DA, Schmidt LD. Synthesis gas formation by direct oxidation of methane over Pt monoliths. *J Catal.* 1992;138:267-282.
5. Hickman DA, Haupfear EA, Schmidt LD. Synthesis gas formation by direct oxidation of methane over Rh monoliths. *Catal Lett.* 1993;17:223-237.
6. Hickman DA, Schmidt LD. Steps in CH_4 oxidation on Pt and Rh surfaces: High-temperature reactor simulations. *AIChE J.* 1993;39:1164-1177.
7. Deutschmann O, Schmidt LD. Modeling the partial oxidation of methane in a short-contact-time reactor. *AIChE J.* 1998;44:2465-2477.
8. Hohn KL, Schmidt LD. Partial oxidation of methane to syngas at high space velocities over Rh-coated spheres. *Appl Catal A Gen.* 2001;211:53-68.
9. Deutschmann O, Schwiedernoch R, Maier LI, Chatterjee D. Natural gas conversion in monolithic catalysts: Interaction of chemical reactions and transport phenomena. Number 136. In Iglesia E, Spivey JJ, Fleisch TH, eds. *Studies in Surface Science and Catalysis: Natural Gas Conversion VI*. Amsterdam, The Netherlands: Elsevier Scientific; 2001:251-258.
10. Schwiedernoch R, Tischer S, Correa C, Deutschmann O. Experimental and numerical study on the transient behavior of partial oxidation of methane in a catalytic monolith. *Chem Eng Sci.* 2003;58:633-642.
11. Tavazzi I. *Short Contact Time Catalytic Partial Oxidation of Methane over Rh/α-Al_2O_3: A Kinetic Study*. PhD Thesis. Milan, Italy: Politecnico di Milano; 2005 (Available at http://www.biblio.polimi.it/opac)
12. Bruno T, Beretta A, Groppi G, Roderi M, Forzatti P. A study of methane partial oxidation in annular reactor: Activity of Rh/α-Al_2O_3 and Rh/ZrO_2 catalysts. *Catal Today.* 2005;99:89-98.
13. Tavazzi I, Beretta A, Groppi G, Fozatti P. An investigation of methane partial oxidation kinetics over Rh-supported catalyst. Number 147. In Bao X, Xu Y, eds. *Studies in Surface Science and Catalysis: Natural Gas Conversion VII*. Amsterdam, The Netherlands: Elsevier Scientific; 2004:163-168.
14. Tavazzi I, Beretta A, Groppi G, Forzatti P. Development of a molecular kinetic scheme for methane partial oxidation over a Rh/α-Al_2O_3 catalyst. *J Catal*. 2006;241:1-13.
15. Maestri M, Beretta A, Groppi G, Tronconi E, Forzatti P. Comparison among structured and packed-bed reactors for the catalytic partial oxidation of CH_4 at short contact times. *Catal Today.* 2005;105:709-717.
16. Bizzi M, Basini L, Saracco G, Specchia V. Modeling a transport phenomena limited reactivity in short contact time catalytic partial oxidation reactors. *Ind Eng Chem Res.* 2003;42:62-71.
17. Leclerc CA, Redenius JM, Schmidt LD. Fast lightoff of millisecond reactors. *Catal Lett*. 2002;79:39-44.
18. Basini L, Marchionna M, Rossigni S, Sanfilippo D. *Catalytic System and Process for Producing Synthesis Gas by Reforming Light Hydrocarbons with CO_2*. U.S. Patent No. 5 336 655; 1994.
19. Valentini M, Groppi G, Cristiani C, Levi M, Tronconi E, Forzatti P. The deposition of γ-Al_2O_3 layers on ceramic and metallic supports for the preparation of structured catalysts. *Catal Today.* 2001;69:307-314.
20. Yoshida F, Ramaswami D, Hougen OA. Temperatures and partial pressures at the surfaces of catalyst particles. *AIChE J.* 1962;8:5-11.
21. Ergun S. Fluid flow through packed columns. *Chem Eng Prog.* 1952;48:89-94.
22. Specchia V, Baldi G, Sicardi S. Heat transfer in packed bed reactors with one phase flow. *Chem Eng Commun.* 1980;4:361-380.
23. Froment GB, Bischoff KB. *Chemical Reactor Analysis and Design*. New York, NY: Wiley; 1990.
24. Wei J, Iglesia E. Structural requirements and reaction pathways in methane activation and chemical conversion catalyzed by rhodium. *J Catal.* 2004;225:116-127.

Manuscript received Feb. 14, 2006, and revision received May 22, 2006.